Combining Finger Vision and Optical Tactile Sensing:
Reducing and Handling Errors While Cutting Vegetables

Akihiko Yamaguchi[1] and Christopher G. Atkeson[1]

***Abstract*— We develop a novel optical multimodal-sensing skin for fingers of a robotic gripper. This sensor consists of a transparent skin made with a marked soft elastic outer layer on a hard layer, and internal RGB cameras. The cameras can see the external scene through the skin. This sensor provides a contact force field estimated by tracking the markers, and visual information of close or grasped objects. This sensor uses off-the-shelf materials, is easy to manufacture, and is robust against an external force as the force is not applied to the sensing device (camera). We install a prototype of this sensor on fingers of a Baxter robot, and demonstrate its usefulness with a cutting vegetable task. The sensor gave us a force information to control cutting vegetables and avoiding slippage of the knife.**

I. Introduction

We are exploring whole-body vision as a sensing skin for human-safe and improved robot control. Different types of sensors are useful to maintain human safety, such as proximity sensors and contact sensors. These sensors are also useful in robust robot control. For example in the DARPA Robotics Challenge Finals, no robots used railings, walls, door frames, or obstacles to support the robot body [1]. Whole-body contact sensors are useful to do this. We are proposing to cover the robot body with a transparent soft material (skin) and put cameras inside (Fig. 1(a)). Such whole-body vision will give us multimodal information such as a proximity (by stereo vision), visual information (color, texture), and contact force estimation (by detecting the skin deformation). This project is named "Argus": Argus Panoptes was a 100-eyed giant in Greek mythology.

This paper focuses on a sensing skin for robotic grippers (Fig. 1(b)). We design the sensing skin for manipulation tasks as well as grasping. We focus on a cutting task with a knife. During cutting, sometimes a strong force is applied to the knife when cutting a hard material, which causes the knife to slip or damage to the fingers. Sensing skin is useful in such a situation providing contact force estimations for avoiding slippage and damage to the fingers, and visual information for slippage detection.

There are many similar approaches to make a tactile sensor with a transparent skin and an imaging sensor inside (e.g. [2], [3], [4], [5], [6], [7]), but all of them are focusing on tactile sensing only, i.e. contact point location and/or contact force/pressure. Most of them are covering the skin surface with opaque material to shut out external light. We think transparent skin gives us richer information.

[1]A. Yamaguchi and C. G. Atkeson are with The Robotics Institute, Carnegie Mellon University, 5000 Forbes Avenue, Pittsburgh PA 15213, United States info@akihikoy.net

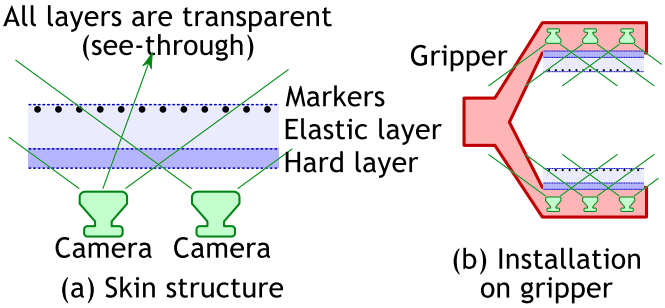

Fig. 1. Conceptual design of our optical multimodal-sensing skin and the installation example on a robotic gripper.

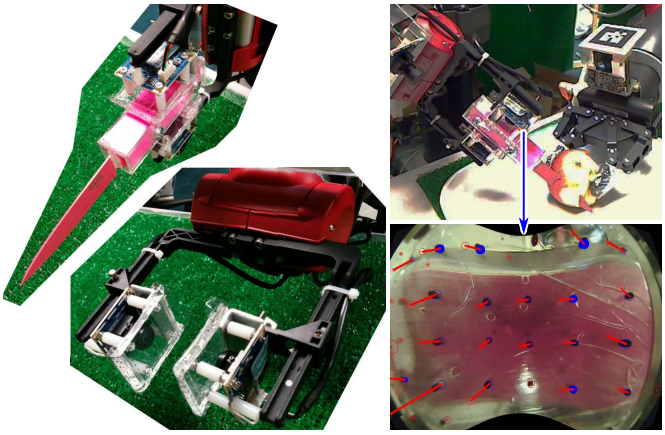

Fig. 2. Prototype of the optical multimodal-sensing skin on the fingers of the Baxter robot. Bottom-left: the sensing skin and the fingers. Top-left: grasping a knife with the sensing skin. Top-right: cutting an apple. Bottom-right: a camera view during cutting where the marker movements are rendered.

In this paper, we make a prototype of the sensing skin. It consists of a camera, a transparent hard layer made with acrylic, a transparent soft layer made with silicone rubber, and colored markers embedded near or on the surface of the soft layer. The markers are used to help detecting the skin deformation. A computer vision method is developed for tracking the markers in order to estimate contact forces. We integrate the sensing skin on the gripper of a Baxter robot, and investigate its usefulness in a practical situation, cutting vegetables with a knife (Fig. 2).

The features of our sensing skin are as follows. It is comparably low cost; it just uses off-the-shelf materials. It is easy to make. The issue is the size reduction; the bottle necks are cameras and lenses. Recently small cameras are widely

developed for various purposes including smart phones. For example in [8], a human fingertip-size device was made with a tiny camera. Our sensing skin is multimodal and it gives us higher resolution of contact forces and proximity vision. It is physically robust because the sensing element (camera) is separated from the skin. We assume that the sensing skin is installed on a robot by fixing the hard layer on a rigid part of the robot. Thus the external force is applied to the soft and hard layers only.

Related Work

The idea of using imaging sensors for tactile sensing is decades old. An initial attempt was measuring the frustration of total internal reflection within a waveguide on a sensor surface caused by contact [2], [3], [9], [10]. The research trend has shifted to measuring displacement of markers placed on the sensor surface with computer vision [4], [5], [11], [12], [13], [6], [14], [7]. A reason would be the marker displacements are proportional to the external force as the displacements are directly caused by the external force. The resolution of the contact force field is decided by the camera and the marker density. Recently high resolution sensors are proposed (e.g. [15], [7]). Another idea is markerless localization of a registered object (e.g. [15]). Such an idea does not require markers. The localization accuracy is ideally equal to the camera resolution. A drawback is the requirement of registering an object. Much of the above work uses a transparent elastic material between the sensor surface and the base. The dynamic range of the force measurement can be controlled by changing the hardness of the elastic material (softer is more sensitive; cf. [16]).

Our research is close to this approach. An important difference is the transparency of the skin including the surface, which gives us richer and multimodal information. Previous work uses opaque surfaces to block the external light as it would affect marker tracking. We solve the marker tracking problem under natural external scenes by computer vision in order to make use of the transparent skin.

Another sensor with transparent skin is proposed in [17] where distance sensors are used instead of a camera. The idea is measuring distances between the sensors and an object, and estimating the deformation of the transparent skin from the distance map. Vertical contact forces are estimated from the deformation. If there is no contact with an object, this sensor simply gives the distance information to a close object. Although this sensor and ours have different sensing modalities and ranges, we would be able to share ideas; e.g. we can embed distance sensors around the cameras.

Many of related research uses a hemisphere shape for fingertip [3], [5], [11], [9], [18], [13], [6], [14], [7], [16], [10], [19]. Their intention is making fingertips of robotic hands or grippers. More human-like fingertips are also proposed (e.g. an elliptical shape [12]). The surface shape should be decided by the task. Although there is research on other shapes such as a flat shape (e.g. [2], [4], [15]), the surface shape requirements have not been studied enough in the context of application tasks. The applications of optical tactile sensors are: grasping task (e.g. [9]), estimating the surface shape or edge of a contacting object (e.g. [13], [18], [14]), and manipulation (e.g. rolling a cylinder [19]). In [10], the sensor is used in a physical human-robot interaction task (passing an object from the robot to a human). In [15], the sensor is used in an insertion task of small parts (e.g. a USB connector into a mating hole). We explore a flat surface and tis usefulness in a cutting task.

II. Optical Multimodal-Sensing Skin for Robot Fingers

A. Overview

The conceptual design of the optical multimodal-sensing skin is shown in Fig. 1. Unlike other research [4], [6], [7], we do not place an opaque material on the surface. The whole skin is transparent except for the markers, and the cameras can see the external scene through the skin.

The markers are captured by the cameras and tracked. This gives us a 3-axis (x,y,z) force measurement at each marker point. By combining multiple marker measurements, we can estimate torque information. In general, a bigger marker is easier to detect; the marker size affects the accuracy of tracking. The density of the markers determines the resolution of the contact force field. There is a trade-off between the resolution and the surface transparency. The hardness and the thickness of the elastic layer affect the marker movement caused by contact force (a softer layer is more easily deformed by a small force), and determine the dynamic range of the contact force measurement. The hard layer is assumed to be fixed on the gripper so that the external force is applied to the elastic and hard layers only and does not affect the cameras. The physical robustness of the sensing skin is decided by the elastic and the hard layers. The camera resolution affects the accuracy of the marker detection and tracking. The camera frame rate affects the sensing frame rate. These properties (the marker size and density, the hardness and the thickness of the elastic and the hard layers, and the camera properties) should reflect the purpose (task) of each part of the skin.

B. Prototype Module of Optical Multimodal-Sensing Skin

We make a prototype module of the optical multimodal-sensing skin for the parallel gripper of a Baxter robot. For simplicity, we use one camera for each finger.

Fig. 3 shows the prototype module and its installation on the Baxter gripper. The size of the module is about 40 mm (W) x 47 mm (L) x 30 mm (H) including a camera module with a USB interface. In the following, we describe the details of making the module.

1) See-through Skin with Markers: Fig. 4 shows a process to make the see-through skin with markers. First we make a mold for the elastic layer. The fingertip edge has a rounded shape; the other part is flat. Then we put markers on the bottom of the mold. We use micro plastic beads of black color for markers, that are spheres of around 1 mm diameter. The markers are placed on a 5 mm grid. We pour silicone rubber into the mold. We use Silicones Inc. XP-565 that

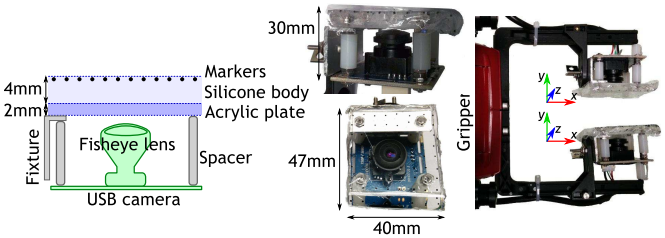

Fig. 3. Prototype module of the optical multimodal-sensing skin (a,b) and its installation on the Baxter gripper.

Fig. 4. Process of making the see-through skin.

has A-16 Shore hardness after cure. Degassing the silicone was important to keep the transparency before pouring the silicone into the mold. Right after pouring into the silicone, we put an acrylic plate (40 mm x 40 mm, 2 mm thickness) with screws as shown in Fig. 4(c). These screws are for preventing the acrylic plate sinking into the silicone, and creating a space for screw heads when attaching the skin to the camera. The thickness of the silicone layer is 4 mm. Fig. 4(d) shows the silicone layer with the acrylic plate after curing. Finally we cover the skin with a thin transparent plastic film (Glad ClingWrap) to protect the silicone skin from dirt. This film is replaceable.

2) Adding a Camera: We attach the camera to the skin. The camera is ELP Co. USBFHD01M-L180 which is an RGB camera with a USB interface and a 180 degree fisheye lens. This skin module works as a stand-alone USB sensor. The lens is adjusted to focus on the markers, which improves the marker tracking quality. We embed a fixture used for integrating into the Baxter gripper in the skin. The fixture is a L-shaped aluminum plate whose one edge is fixed on the acrylic plate (see Fig. 3(a)). Fig. 3(b) shows the side and top views of the module. In the top view, we can see the camera through the skin; thus the silicone and acrylic layers have good transparency.

C. Installation to Gripper Fingers of Baxter Robot

The gripper of the Baxter robot is a parallel gripper with two fingers. We made two prototype modules and attach one for each finger. We create a simple mount for the sensor as shown in Fig. 3(c).

D. Marker Tracking for Contact Force Estimation

We use an existing blob detection method for markers implemented in OpenCV[1], `cv::SimpleBlobDetector`, that detects small blobs from an image. Each detected blob has a position (x,y) and size in the image.

Since the camera image is distorted due to the fisheye lens, we rectify the input image before detecting the blobs. We use calibration methods from OpenCV.

Our marker tracking algorithm is simple. First we calibrate the marker tracker by obtaining the initial marker positions and sizes. In each frame, we compare the current marker positions and sizes with the initial markers.

1) Marker tracker calibration: We use 20 frames for marker tracker calibration where we put a white board on the skin so that the blob detector detects only the markers. If there are moving blobs, they are rejected. We take an average of the remaining blob positions and sizes and keep them as the initial markers.

2) Marker tracking: In each frame, we detect blobs from an input image, and compare them with the initial markers. Since the order of the blobs does not correspond with the initial markers, we assume the closest blob to a blob in the initial frame is the same marker. We define thresholds on position and size differences, and if they are too large, we reject them. For each marker position and size differences dx, dy, ds, we estimate the contact force $\mathbf{f}$ as:

$$\mathbf{f} = [c_x dx, c_y ds, c_z dy] \quad (1)$$

where c_x, c_y, c_z are conversion coefficients (refer to Fig. 3(c) for the coordinate definition). These coefficients are for human readability, not for converting to regular units such as Newtons.

We can use these contact force estimates as a force field estimate. We can also convert them to an average force and torque, which would be useful for simple applications. For this, we first define a torque estimate around the center of the skin surface as: $\boldsymbol{\tau} = c_\tau \mathbf{r} \times \mathbf{f}$, where $\mathbf{r}$ is a displacement vector from the center of the skin surface to the marker, and c_τ is a conversion coefficient. For averaging $\mathbf{f}$ and $\boldsymbol{\tau}$, we use the element-wise 80th percentile[2] of the absolute value. This filter gives us a robust estimation against the outliers in the marker tracking, and picks up a local force when the external force is applied to a narrow region of the skin surface.

We programmed the above methods with as many threads as possible. The whole process including capturing from cameras is computed in around 30 frames per second with two cameras whose resolution is 640x480. The computer has an Intel Core i7 CPU (2.70 GHz, 4 cores, 8 hyper threads) and 16 GB RAM.

III. Experiments

We demonstrate our sensing skin in some experiments. In these experiments we do not apply a temporal filter, which

[1] `http://opencv.org/`

[2] Using the value splitting the highest 20% of the data from the lowest 80%.

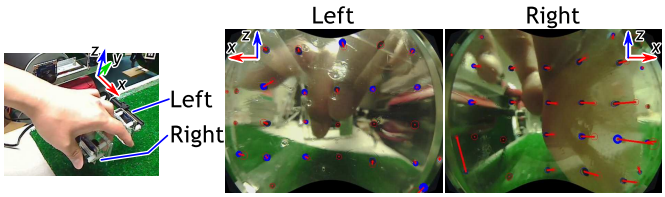

Fig. 5. Pushing force by a human. The right two images are views from the cameras. The marker movements are rendered (the movements are emphasized).

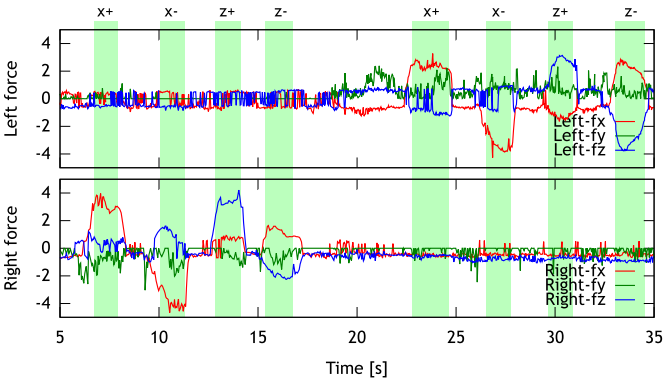

Fig. 6. Trajectories of the average force (x,y,z) of the left (top graph) and the right (bottom graph) sensing skins during pushing by a human.

should be need to further reduce noise and errors. Refer to the accompanying video.

A. Pushing Force Directly Applied to The Skin

First, we let a human push the skin horizontally (x and z axes) for each finger respectively. Fig. 5 shows a captured image (rectified) with a visualization of the marker movements. We can see that the markers are moved, and can see the human fingers through the skin. Fig. 6 shows the trajectories of the average force (x,y,z) of the left and the right sensing skins. In both sides, the horizontal (x and z) forces are changing towards pushed directions. During pushing, the vertical (y) force is changing slightly, but is noisy. This is because the vertical force is estimated from the marker size change and the size does not change much compared to the horizontal marker displacement. The reason why the value of the left sensor is changing around 20 sec is that the human finger is contacting the skin.

B. Pushing Force Applied to Holding Knife

We make the robot hold an knife and let a human push and pull the knife in various directions as shown in Fig. 7. Fig. 8 shows the trajectories of the average force (x,z) and torque (y) of the left and the right sensing skins. Each sensor value has an offset value since the gripper is holding the knife. The horizontal pushing (tx+, tx−) are captured by the x-force value of the left sensor, while the second tx− (around 14 sec) is hardly detected by the right sensor. The reason would be that the surfaces of the sensors were not completely parallel due to an inaccurate construction, which probably caused

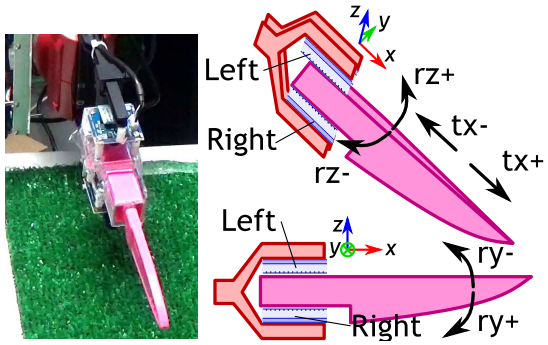

Fig. 7. Experimental setup of pushing a knife held by the gripper. Pushing directions are illustrated.

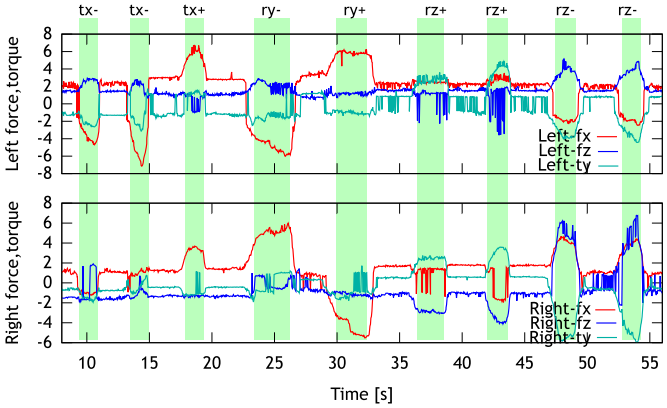

Fig. 8. Trajectories of the average force (x,z) and torque (y) of the left and the right sensing skins during pushing the knife.

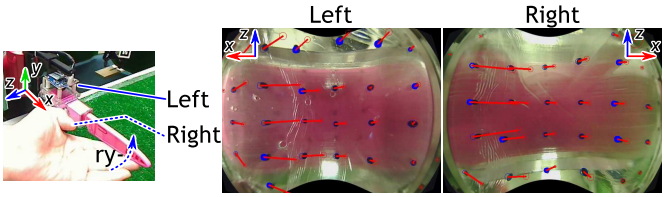

Fig. 9. Marker tracking result in pushing in the ry− direction (vertical rotation). The left image is a view from an external camera.

an asymmetric force distribution. The vertical rotational-pushing (ry+, ry−) are detected clearly by the x-force values of both sensors which have opposite directions because of the torque applied to the knife. Fig. 9 shows the marker tracking result in ry−. The y-torque value captures the horizontal rotational-pushing (rz+, rz−), however it seems to have a large hysteresis.

C. Force Profile of Cutting Motion by Human

Next, we let a human hold a knife with the sensing skins. For this purpose, we detach the fingers from the robot and let the human hold the entire finger with the knife as shown in Fig. 10. The human cuts a banana and an apple. Fig. 11 shows the trajectories of the average force (x,z) and torque (y) of the left and the right sensing skins. The first half is cutting a banana several times, and the last half is cutting

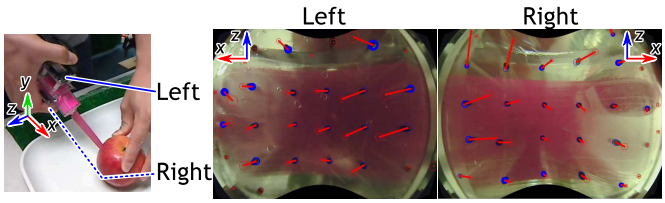

Fig. 10. Setup of the cutting motion by a human. The human holds the sensors with a knife, and cuts materials. The left view shows an example of cutting an apple, and the right two images are views of the sensing skins.

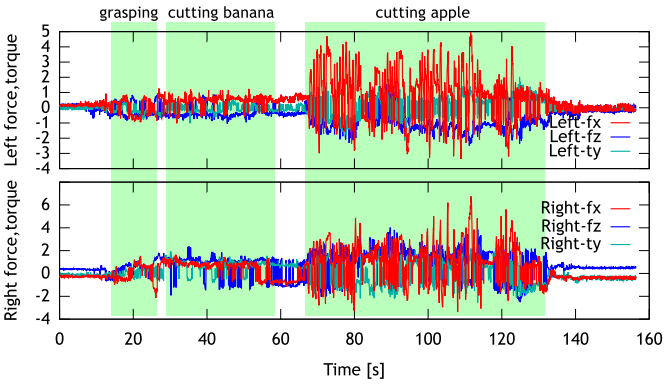

Fig. 11. Trajectories of the average force (x,z) and torque (y) of the left and the right sensing skins during cutting a banana and an apple by the human. In the first short period, the human grasped the knife, and then cut the banana and the apple.

an apple. There is a significant difference between cutting the apple and banana. There are subtle sensor value changes during cutting the banana because of the softness of banana. The human cut the apple with "sawing" while the banana was cut by just pushing the knife down.

D. Robotic Cutting Motion with Sensing Skin

We implemented an automatic cutting motion with the sensing skin. Through our preliminary experiments where we controlled the robot manually with a joy stick controller, we found these difficulties: (1) When cutting a hard material, a strong vertical force was applied to the knife, which deformed the grasp (cf. Fig. 12(a)). (2) When a force was applied to the knife horizontally, the knife slipped in the gripper (cf. Fig. 12(b)). In this experiment, we show that using our sensing skins, we can easily make a controller to avoid these difficulties. Note that even if (1) or (2) happens, the visual views through the skin tell us something happened. For example, look at the camera view of Fig. 12(b); we can find that the angle of the knife is different from its initial grasp position.

We created a cutting controller which (a) starts from a state where the knife held by the gripper is put above the material, (b) moves the knife downward (cutting vertically), and then (c) slightly pulls the knife (cutting horizontally). The controller moves the knife to the initial position in order to repeat the motion several times. The difficulties (1) and (2) might happen in the step (b). To avoid them, we consider

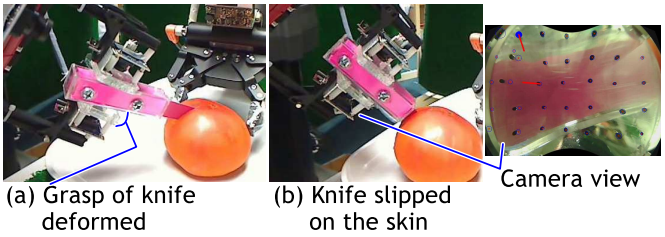

Fig. 12. Difficulties in cutting.

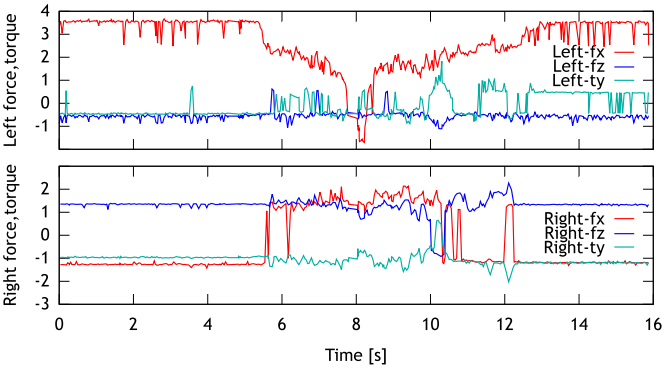

Fig. 13. Trajectories of the average force (x,z) and torque (y) of the left and the right sensing skins during cutting a banana by the robot. There was a single cutting motion around the peak of left x-force.

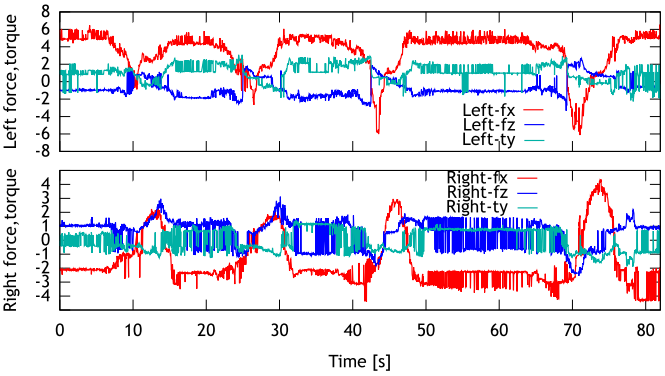

Fig. 14. Trajectories of the average force (x,z) and torque (y) of the left and the right sensing skins during cutting an apple by the robot. The robot performed the cutting motion four times to cut the apple completely. The peaks of left and right x-force correspond with the cutting motion.

conditions to stop the motion: (A) if $-(f_{\mathrm{L}x} - f_{\mathrm{L}x0})(f_{\mathrm{R}x} - f_{\mathrm{R}x0}) > 10$, or (B) if $|\tau_{\mathrm{L}y}| + |\tau_{\mathrm{R}y}| > 4$, where $f_{\mathrm{L}x}$ and $f_{\mathrm{R}x}$ indicate the x-value of the average force of the left and the right sensors, $f_{\mathrm{L}x0}$ and $f_{\mathrm{R}x0}$ indicate their initial values (right before cutting), and $\tau_{\mathrm{L}y}$ and $\tau_{\mathrm{R}y}$ indicate the y-value of the average torque of the left and the right sensors. The condition (A) is defined according to the result of ry− in Section III-B where the vertical force was applied to the knife. The condition (B) helps to avoid rotational knife slip.

Fig. 13 and Fig. 14 shows the sensor values during cutting a banana and an apple respectively where the trajectories of the average force (x,z) and torque (y) of the left and the right sensing skins are shown. Since cutting a banana requires only

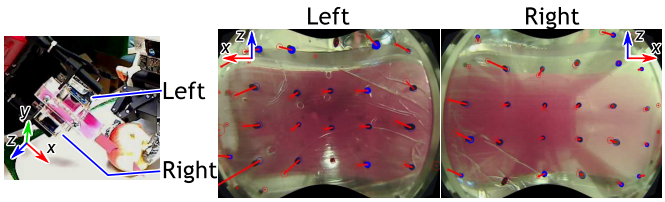

Fig. 15. Marker tracking result in cutting an apple by the robot. The left image is a view from an external camera.

a small force, the robot cut it with a single trial, while the robot took four trials in cutting an apple. In the banana case, the robot stopped moving the knife because the condition (A) was satisfied as the knife hit the cutting board. In the apple case, the condition (A) was mainly satisfied by the pressure from the cut edge of the apple fresh. In these graphs, the condition (B) was not satisfied, but it was useful when the initial knife orientation was not perpendicular. Fig. 15 shows a marker tracking result in cutting an apple. Although the cutting motion is simple, it was capable to cut materials while avoiding the above difficulties (1), (2).

IV. Discussion

1) Should we convert the force estimate to an engineering unit (e.g. Newtons)?: This depends on the application. We are planning to use machine learning methods to learn the dynamical models (relation between input gripper motion and output force changes) for example by using neural networks [20]. In such a case, obtaining contact force information in engineering units is not necessary. Consistent estimates are important. However using an engineering unit will be generalizable to other situations and other robots, so it will be still useful.

2) Accuracy, reliability, and hysteresis: Although we did not conduct a controlled evaluation, the horizontal force seems to be reliable. The marker movement in a horizontal direction is easier to track. The vertical force seems to be more difficult to detect as the changes of the marker visual size are comparably smaller. Perhaps we can use the vertical force estimate as an on/off signal. A way to improve the vertical force accuracy is increasing the thickness of the elastic layer, although it would make the skin heavier.

In the experiments, there were some false detections of the markers. These were mostly due to the external scene. Increasing the number of markers is helpful for removing outliers, although it will reduce the transparency accordingly. Putting an internal light source would be helpful in dark scenes.

We found hysteresis, especially when a strong force was applied. In the cutting vegetable experiments by the robot, the force estimate changed before and after cutting a hard material. This would be because the deformation of the soft layer remained. This was mostly reset after releasing the knife.

3) Calibration frequency: During the experiments of the previous section, we did the calibration of the marker tracking only twice. The first one was the initialization. The second one was necessary due to the accidental separation of the soft layer and the acrylic base.

4) Physical robustness: A weak part of the sensor is the adhesion between the soft skin and the acrylic base. Currently we rely on the sticky property of the silicone rubber. It was strong enough against horizontal forces and downward forces from above, but the skin can be easily peeled by upward forces from below. This issue would be solved by an adhesive between the layers.

Other than that, the sensor strength is decided by the acrylic base hardness and the soft skin. For heavier tasks where larger contact forces will be applied, we would need a thicker acrylic base. Although the soft skin is weak against something with thin tips (e.g. needle) or sharp edges (e.g. knife), the hardness is close to that of the human skin. Thus we think it is strong enough for daily manipulations.

V. Conclusion

We developed an optical multimodal-sensing skin for robot fingers. The sensor structure is simple: a transparent skin made with a marked soft elastic outer layer on a hard layer, and internal RGB cameras. The important feature is the see-through skin that provides visual information of a close object. We installed a prototype of the sensor on fingers of a Baxter robot, and used it in a practical task, cutting vegetables. The sensor gave us a force estimate to control cutting vegetables and avoiding slippage of the knife.

References

[1] C. Atkeson *et al.*, "NO FALLS, NO RESETS: Reliable humanoid behavior in the DARPA Robotics Challenge," in *the 15th IEEE-RAS International Conference on Humanoid Robots (Humanoids'15)*, 2015.

[2] S. Begej, "Planar and finger-shaped optical tactile sensors for robotic applications," *IEEE Journal on Robotics and Automation*, vol. 4, no. 5, p. 47200484, 1988.

[3] H. Maekawa, K. Tanie, K. Komoriya, M. Kaneko, C. Horiguchi, and T. Sugawara, "Development of a finger-shaped tactile sensor and its evaluation by active touch," in *Robotics and Automation, 1992. Proceedings., 1992 IEEE International Conference on*, vol. 2, 1992, pp. 1327–1334.

[4] K. Kamiyama, H. Kajimoto, N. Kawakami, and S. Tachi, "Evaluation of a vision-based tactile sensor," in *Robotics and Automation, 2004. Proceedings. ICRA '04. 2004 IEEE International Conference on*, vol. 2, 2004, pp. 1542–1547.

[5] J. Ueda, Y. Ishida, M. Kondo, and T. Ogasawara, "Development of the NAIST-Hand with vision-based tactile fingertip sensor," in *Proceedings of the 2005 IEEE International Conference on Robotics and Automation*, 2005, pp. 2332–2337.

[6] Y. Ito, Y. Kim, and G. Obinata, "Robust slippage degree estimation based on reference update of vision-based tactile sensor," *IEEE Sensors Journal*, vol. 11, no. 9, pp. 2037–2047, 2011.

[7] N. F. Lepora and B. Ward-Cherrier, "Superresolution with an optical tactile sensor," in *Intelligent Robots and Systems (IROS), 2015 IEEE/RSJ International Conference on*, 2015, pp. 2686–2691.

[8] X.-D. Yang, T. Grossman, D. Wigdor, and G. Fitzmaurice, "Magic finger: Always-available input through finger instrumentation," in *Proceedings of the 25th Annual ACM Symposium on User Interface Software and Technology*, 2012, pp. 147–156.

[9] H. Yussof, J. Wada, and M. Ohka, "Sensorization of robotic hand using optical three-axis tactile sensor: Evaluation with grasping and twisting motions," *Journal of Computer Science*, vol. 6, no. 8, pp. 955–962, 2010.

[10] T. Ikai, S. Kamiya, and M. Ohka, "Robot control using natural instructions via visual and tactile sensations," *Journal of Computer Science*, vol. 12, no. 5, pp. 246–254, 2016.

[11] C. Chorley, C. Melhuish, T. Pipe, and J. Rossiter, "Development of a tactile sensor based on biologically inspired edge encoding," in *Advanced Robotics, 2009. ICAR 2009. International Conference on*, 2009, pp. 1–6.

[12] D. Hristu, N. Ferrier, and R. W. Brockett, "The performance of a deformable-membrane tactile sensor: basic results on geometrically-defined tasks," in *Robotics and Automation, 2000. Proceedings. ICRA '00. IEEE International Conference on*, vol. 1, 2000, pp. 508–513.

[13] Y. Ito, Y. Kim, C. Nagai, and G. Obinata, "Shape sensing by vision-based tactile sensor for dexterous handling of robot hands," in *2010 IEEE International Conference on Automation Science and Engineering*, 2010, pp. 574–579.

[14] T. Assaf, C. Roke, J. Rossiter, T. Pipe, and C. Melhuish, "Seeing by touch: Evaluation of a soft biologically-inspired artificial fingertip in real-time active touch," *Sensors*, vol. 14, no. 2, p. 2561, 2014.

[15] R. Li, R. Platt, W. Yuan, A. ten Pas, N. Roscup, M. A. Srinivasan, and E. Adelson, "Localization and manipulation of small parts using gelsight tactile sensing," in *2014 IEEE/RSJ International Conference on Intelligent Robots and Systems*, 2014, pp. 3988–3993.

[16] OptoForce Co., "White paper: Optical force sensors — introduction to the technology," Tech. Rep., January 2015. [Online]. Available: http://optoforce.com/

[17] R. Patel and N. Correll, "Integrated force and distance sensing using elastomer-embedded commodity proximity sensors," in *Proceedings of Robotics: Science and Systems*, 2016.

[18] S. C. Abdullah, J. Wada, M. Ohka, and H. Yussof, "Object exploration using a three-axis tactile sensing information," *Journal of Computer Science*, vol. 7, no. 4, pp. 499–504, 2011.

[19] L. Cramphorn, B. Ward-Cherrier, and N. F. Lepora, "Tactile manipulation with biomimetic active touch," in *2016 IEEE International Conference on Robotics and Automation (ICRA)*, 2016, pp. 123–129.

[20] A. Yamaguchi and C. G. Atkeson, "Neural networks and differential dynamic programming for reinforcement learning problems," in *the IEEE International Conference on Robotics and Automation (ICRA'16)*, 2016.